Long-term Geomagnetic Indices and their Use in Inferring Solar Wind Parameters in the Past

L. Svalgaard, Easy Toolkit, Inc, 6927 Lawler Ridge, Houston, TX 77055, USA.
[leif@leif.org]

E. W. Cliver, Space Vehicles Directorate, Air Force Research Laboratory, Hanscom AFB, MA 01731, USA.
[Edward.Cliver@hanscom.af.mil]

Abstract

We discuss three new geomagnetic indices [the Inter-Hour Variability (*IHV*), Svalgaard and Cliver (2007); the Inter-Diurnal Variability (*IDV*), Svalgaard and Cliver, 2005; and the Polar-Cap Potential (*PCP*) Index, Le Sager and Svalgaard (2004)], that are derivable from data available for a century or more. Each of these indices responds directly to either the solar wind magnetic field strength (*B*) or to different combinations of *B* and the solar wind speed (*V*). This over-determined system permits a reconstruction of these parameters for the past ~150 years. The variation of yearly averages of *B* can be described as a constant value (4.6 nT) plus a component varying with the square-root of the sunspot number. Because the latter seems to exhibit a ~100 year Gleissberg cycle, *B* does as well. Since 1890, annual averages of *V* range from a low of ~300 km/s in 1902 to 545 km/s in 2003. The *IHV*-index fords a way to check the calibration of other long-term geomagnetic indices. We find that the *ap*-index tracks the variation of *IHV*, back to 1932 but that the *aa*-index (extended back to 1844) is systematically too low (3-6 nT) before 1957, relative to modern values.

1. Geomagnetic Activity Indices

Geomagnetic activity results from the interaction (compression and magnetic reconnection) between the solar wind and the magnetosphere. It is characterized by geomagnetic indices (Mayaud, 1980), which are driven by some combination of the following solar wind variables and system parameters:

1. The interplanetary magnetic (*B*) flux per unit time and area, $B\,V$
2. The solar wind momentum ($nm\,V$) flux per unit time and area, ($nm\,V$) V
3. The angles between the Earth's magnetic field and the IMF direction (α) and flow direction (ψ)
4. The time scale of interest (hours to days) and the variability within that

2. Analysis of the *am*-index

We shall review an analysis of a well-established activity index: the *am*-index defined by Mayaud (1967, 1968), and then transition to our own *IHV*-index (Svalgaard et al., 2003; Svalgaard et al., 2004) covering a much longer time interval. A common technique in laboratory physics is to keep all variables nearly constant except one and investigate the effect of varying only that one. We will follow this approach here to determine the effect of the various solar wind parameters given in (`http://omniweb.gsfc.nasa.gov`). The difference in time resolution (1 hour for the solar wind data and 3 hours for the *am*-index) is matched by averaging the shorter time resolution into the longer one. The details of the analysis can be found in Svalgaard (1977).

We first varied only the IMF strength, keeping *V* in a narrow interval. Similarly, the number density, *n*, was kept in a narrow interval (assuming that the mass, *m*, per particle is approximately constant) and the variability (see below) as well. The values chosen correspond to average solar wind conditions. The *am*-index was found to vary with the first power of *B* both all merging angles, with the activity level much larger for Southward angles ($\cos\alpha < 0$). Repeating the analysis for other (narrow) intervals of solar wind speed *V* gave essentially the same

result. This suggests that we can eliminate the influence of BV by dividing am by BV. We shall often use the abbreviation V_o for V/100 km/s. The '~' symbol in this paper means 'equal to within a constant (possibly including a small offset)' or 'approximately equal to', depending on context.

Determining activity (reduced by BV) for narrow bins of the momentum flux per unit mass, nV^2 we found that we can eliminate the influence of the solar wind momentum flux by dividing by the cube-root of nV^2:

$$am' = am\ (<BV>/BV)\ (<nV^2>/nV^2)^{1/3}$$

where <…> denotes the average value.

The am-index is a three-hour index and during that interval the IMF can vary significantly (mostly in direction). We express the variability of the IMF by the ratio

$$f = (\sigma_{BX}^2 + \sigma_{BY}^2 + \sigma_{BZ}^2)^{1/2}/B$$

The efficiency of the coupling between the solar wind and the magnetosphere depends on the merging angle α, but also critically on the variability, f. When $f = 1$, there is no real dependence on α as the field varies randomly within the time interval, but for $f = 0$, there is a strong effect of steady southward fields (cos α < 0). The coupling function of f and cos α can be modeled by an exponential

$$q\ (f, \cos\alpha) \sim \exp[-p_4\ (f, \cos\alpha)]$$

where the argument, p_4, is a fourth-order polynomial fit to f and cos α. This relationship is, of course, purely empirical and aims only at a (as it turns out, fairly accurate) *description* of the dependence. We can then write

$$am \sim BV\ (nV^2)^{1/3}\ q\ (f, \cos\alpha)$$

With this relationship we can now ***calculate*** the am-index values from solar wind parameters.

The analysis described above was actually first carried out 30 years ago using the first solar cycle's worth of interplanetary data (Svalgaard, 1977). Our recent analysis of three additional cycles fully confirms the early results. Figure 1 shows computed and observed am-values for individual three-hour intervals through six Bartels rotations. The scale is logarithmic to show that the fit is equally good for both high and low values, except for the very lowest values of am, which are not reliable as they are very difficult to measure. These low values are systematically measured to be too low by 3-5 nT.

For averages over months or years, <cos α> is to first order constant, but <f> is not. At times with high solar wind speed, f is higher too, increasing the coupling efficiency. The net result is that the expression $am \sim Bn^{1/3}V^{5/3}$, that is valid for individual three-hour intervals, for longer-term averages acquires a slightly higher exponent for V, namely V^2. Noting that longer-term averages of $n^{1/3}$ do not vary much, we finally end with the expectation that $\boldsymbol{am \sim BV^2}$ for averages over months or more, and this is indeed what we find. There is thus a quantitative physical basis for the am-index (and other such range indices).

3. The *IHV*-index

The am index is only available since 1959. Similar indices (*ap* and *aa*) go back further but have (possibly) uncertain calibrations and cannot be reproduced. The main (actually the only) difficulty with these indices (or their equivalent *K*-indices) is the identification and removal of the ("irregularly" varying) regular diurnal variation. We attempted to sidestep this difficulty by only using data from the nighttime and define the Inter-Hour Variability index (*IHV*) as the sum of the six *unsigned* differences between hourly (mean) values of a geomagnetic element (for this paper we use the H-component) for the seven-hour interval centered on local

midnight, the fourth hour containing midnight (Svalgaard et al., 2004). Certain phenomena occur chiefly on the dayside of the magnetosphere (e.g. solar flare effects, the 'regular' solar quiet-time thermal wind and tidal effects, sudden storm commencements, the Svalgaard- Mansurov effect) and have physical causes distinct from the 'classical' geomagnetic activity that peaks near midnight.

The *IHV*-index can be automatically derived from 'yearbook' data, which go back to the 1840s. There is a technical matter having to do with the difference between hourly values (instantaneous on the hour mark) and hourly means (mean values over an hour usually centered on the half-hour mark). The latter were introduced by A. Schmidt with the 1905 Potsdam yearbook. Mean values have lower variance and thus lower *IHV*-values. This effect can reach 60%, but can easily be corrected for, once identified in the data. Figure 2 shows monthly means of *IHV* for FRD (blue) compared to monthly means of simultaneous *am* values (thick red curve). The thin pink curve is simply 0.7475 *IHV* and matches the *am*-curve well, suggesting the use of *IHV* as a proxy for *am*.

IHV is a *subauroral* zone index (less than 55˚ corrected geomagnetic latitude) just like *am*. The index shows a dramatic increase for stations above 55˚. Higher-latitude *IHV* reacts differently to solar wind parameters. It is therefore important to limit the application of *IHV* to subauroral stations. Figure 2 shows that even a single station can provide a reliable *IHV* proxy for *am*. To get a global index, we divide the globe into six longitude sectors with each a northern and southern latitude part and combine available stations (normalized to Niemegk, NGK) into an index for each sector. Averaging all sectors gives us a global composite *IHV*-index covering all Universal times and both hemispheres (Svalgaard and Cliver, 2007).

Because the *am*-index varies with BV^2, we expect *IHV* to do the same, and so it does, as shown in Figure 3(a,b). In Figure 3(a) we have turned the correlations around calculating solar wind parameters from geomagnetic activity instead of activity from solar wind parameters. This allows us to estimate solar wind and interplanetary physical quantities using the Earth's magnetosphere as the measuring device.

In Figure 3(b), we have indicated with gray circles) some areas of less agreement between calculated and observed BV_o^2. We attribute these discrepancies to the 22-year cycle (Chernosky, 1966; Russell, 1974; Cliver et. al., 1996) in geomagnetic activity. The circled discrepancies arise from a combination of two effects. The Russell-McPherron effect causes opposite annual variations of southward IMF for the two polarities of the IMF (Russell and McPherron, 1973). During the minimum and rising phases of the solar cycle there is an imbalance between the occurrence of the two polarities (the Rosenberg-Coleman effect, Rosenberg and Coleman, 1969). Because the solar polar fields show a 22-year cycle, the combination of these two effects results in geomagnetic activity being higher every other cycle when the R-C effect is present. The green line shows the size of the R-C effect (in arbitrary units) derived from the observed IMF polarity (Echer and Svalgaard, 2004). We leave these second-order discrepancies in the *IHV*-index with the knowledge that they exist.

Both *am* and (raw) *IHV* show a dependence on the tilt angle of the Earth's dipole towards the solar wind direction (ψ): $am \sim S(\psi) = (1+3\cos^2\psi)^{-2/3}$ (Svalgaard, 1977; Svalgaard et al, 2002; O'Brien and McPherron, 2004; McPherron, 2004). Since the dipole axis is inclined 11˚ to the rotation axis, this dependence, involving the dipole field strength at the subsolar point, introduces an undesirable dependence on longitude. We eliminate this by dividing *IHV* by the function $S(\psi)$. In this way, *IHV*-values from stations at different longitudes can be directly combined. The ψ-dependence is a true modulation of existing activity. It does not depend on the direction of the IMF (Northward or Southwards field).

4. The *IDV*-index

The *IHV*-index captures activity on a time scale of hours. How about on a time scale of days or longer? Bartels (1932) defined his *u*-measure as the monthly (or longer) mean of the unsigned differences between the mean values of the H-component on two successive days. In our study of the interdiurnal variability, we found that the *u*-measure varies little if one uses a mean over a whole day or a few hours, near local midnight, or a single hour at this time. The *IDV* index is thus defined as simply a modern version of the *u*-measure (in nT, not

the original 10 nT units) using only one hour (preferably the midnight hour if available). Neither *u* nor *IDV* registered the strong high-speed streams in 1930, 1952, 1974, 1994, and 2003. The failure to register the very high 1930 activity level was a deadly blow to the *u*-measure, causing Bartels to abandon the index. What *is* the *IDV*-index then measuring? In Figure 4 we plot yearly averages of *B* and *V* against *IDV*: There is indeed no correlation with *V*. There *is* a robust correlation with *B*. Various fits (linear, power law) do not really differ over the range of the data (Svalgaard and Cliver, 2005, 2006).

Coronal Mass Ejections (CMEs) add (mainly closed) magnetic flux to the IMF and also compress the ambient IMF. The resulting strong magnetic fields of CMEs hitting the Earth create magnetic storms, feeding energy into the inner magnetosphere ("ring current"). The *Dst*-index is aimed at describing this same phenomenon, but only the negative contribution to *Dst* on the nightside is effectively involved. Because positive and negative values of *Dst* are due to different physical processes (controlled roughly by solar wind pressure and magnetic reconnection in the magnetotail, respectively) a simple yearly average of *Dst* is a somewhat suspect physical quantity. If we include only negative values of *Dst* in the average, we isolate the effects of magnetic reconnection. We therefore expect (negative) *Dst* and *IDV* to be strongly related, and they are as shown in Figure 5. We used a derivation of *Dst* by J. Love back to 1905 (Love, 2006). Similar results are obtained with the *Dst* series by Karinen and Mursula (2005) back to 1932 or with the "official" *Dst* series, back to 1957. The very simple-to-derive *IDV* series compares favorably with the more elaborate *Dst*(< 0) .Using regressions of *IDV* and *Dst* (< 0) on IMF *B* we can directly estimate *B* back to 1872 with the result shown in Figure 6. There is a hint of a ≈100-year Gleissberg-type cycle.

Can we go further back in time? Bartels had determined the *u*-measure from 1836 on, but with less confidence before 1872. Figure 7b shows what we get if we infer *IDV* (and then *B*) from *u* back to 1836. The smooth curve is a 4^{th}-order polynomial fit. We may be approaching another minimum in the Gleissberg cycle. The IMF *B* for 2007 (so far, through June) is the lowest in the last 106 years. The main sources of the equatorial components of the Sun's large-scale magnetic field are large active regions. If these active regions emerge at random longitudes, their net equatorial dipole moment will scale as the square root of their number. Thus their contribution to the average IMF strength will tend to increase as the square root of sunspot number, R_z, (for a detailed discussion, see Wang and Sheeley, 2003). There is, indeed, such a correlation (Figure 7a; Svalgaard and Cliver, 2005), and we can therefore attempt to infer *B* from R_z as well and compare with *B* inferred from *u* (Figure 7b). Before about 1850, either *u* is too large or R_z is too small. This is problem for further research. Preliminary analysis (Svalgaard and Cliver, 2007) suggests that R_z is too small prior to ~1875.

5. The Polar Cap Potential index

The Hall ionospheric current flowing across the Earth's polar caps (e.g., Ritter et al., 2004) is the source of the last geomagnetic index we will discuss, the Polar Cap Potential (PCP) index. The Earth rotates under this current causing the magnetic effect of the current to rotate once in 24 hours adding a circular motion to the end-point of the horizontal component vector (Le Sager and Svalgaard, 2004). This rotating daily effect is readily (and has been since 1882) observed at polar cap magnetic observatories (Figure 8). The current derives from the Polar Cap Electric Potential which is basically the electric field ($\boldsymbol{E} = -\boldsymbol{V}\mathrm{x}\boldsymbol{B}$) in the solar wind mapped down to the ionosphere.

Figure 9a shows for each year of 1965-2004 how the average radius of the circular variation of the end-point of the horizontal component depends on the product of *B* and *V* for Thule (THL) and for Resolute Bay (RES). The radius of the circular variation is virtually the same for all stations in the cap. The radius of the circle traced out by variation of horizontal component is a measure of the polar cap potential. For stations near the polar cap boundary the circle is only partial. We can then estimate the time variation of *BV* as shown in Figure 9b.

6. Determining solar wind parameters from the indices

We now have three independent ways of estimating solar wind and IMF parameters:

1. The *IHV*-index, estimating BV^2
2. The *IDV*-index, estimating B
3. The *PCP*-index, estimating BV

These indices are readily computed from simple hourly means values for which we have measurements stretching back well into the 19th century. We can thus estimate $V = \sqrt{[(BV^2) / B]}$ and use that value to calculate BV for comparison with the estimated BV. The agreement (Figure 10) is encouraging. There are several second-order effects (22-year cycle, solar cycle variations of ionospheric conductivity, secular decrease of Earth's dipole moment, records going off-scale, etc) that can be compensated for, but the overall picture seems clear already.

7. Cross-checking other long-term indices

We can even use the *IHV*-index as a check on the long-term stability of the *aa*-index (Mayaud, 1972). Regressing *aa* versus *IHV* for recent times we find excellent agreement (Figure 11). Using the regression of Figure 11 we can calculate *aa* under the assumption that the *aa*-index has a calibration that is constant in time. Figure 12 shows the difference between observed and calculated Bartels rotation averages of the *aa*-index since 1890. Note the marked discontinuity at the beginning of the year 1957. It would seem that the *aa*-index is in need of a recalibration. The same conclusion was also reached by Svalgaard et al. (2004), Jarvis (2005), Svalgaard and Cliver (2006b), and Lockwood et al. (2006). A similar analysis for the *ap*-index suggests that this index does not suffer from calibration problems.

8. Geomagnetic activity back to 1844

The analyses and results presented in this review paper underscore the immense value of old geomagnetic records. An effort should be made to preserve that legacy and to bring the data into electronic form. We can then apply the same technique for that early data. Figure 13 shows the result of using the Helsinki observatory data (1844-1897) to extend *IHV* back to 1844. For comparison we also plot (Figure 14) the *ak*-index derived from the same data by Nevanlinna and Kataja (1993) and the *IHV* index scaled to *aa* using the regression of Figure 11. As the *ak*-index was normalized to match the *aa*-index for the time when they overlap it is not surprising that *ak* is also lower (by ~6nT for yearly means) than our *IHV* converted to *aa*. The simplicity and reproducibility of *IHV* compared to *aa* and similar indices might inspire confidence in the long-term calibration of this objective measure of geomagnetic activity.

9. Conclusion

By constructing geomagnetic indices that are directly related to separate physical conditions in the solar wind we bring investigations of the long-term behavior of these conditions onto a firm physical basis and remove much of the speculative character of our inferences about Space Climate. At the same time we are able to bring the historical record of geomagnetic measurements to bear on the issues of Space Climate in ways our predecessors could not dream of, but would certainly much appreciate and delight in.

References

Bartels, J. Terrestrial-magnetic activity and its relations to solar phenomena, Terr. Magn. Atmos. Elec. 37, 1., 1932.

Chernosky, E. J. Double Sunspot-Cycle Variation in Terrestrial Magnetic Activity 1884-1963, J. Geophys. Res. 71, 965, 1966.

Cliver, E.W., Solar activity and geomagnetic storms: The first 40 years, Eos, 75(49), 569, 574-575, 1994.

Cliver, E. W., V. Boriakoff, K. H. Bounar, The 22-year cycle of geomagnetic and solar wind activity, J. Geophys. Res. 101(A12), 27091, 1996.

Echer, E., Svalgaard, L. Asymmetry in the Rosenberg-Coleman effect around solar minimum revealed by wavelet analysis of the interplanetary magnetic field polarity data (1927-2002), Geophys. Res. Lett. 31(12), L12808, doi:10.1029/2004GL020228, 2004.

Jarvis, M. (2005), Observed tidal variation in the lower thermosphere through the 20th century and the possible implication of ozone depletion, J. Geophys. Res. 110, A04303, doi:10.1029/2004JA010921.

Karinen, A., Mursula, K. A new reconstruction of the Dst index for 1932-2002, Ann. Geophys. 23(2), 475-485, 2005.

Le Sager, P., Svalgaard, L. No increase of the interplanetary electric field since 1926, J. Geophys. Res. 109(A7), A07106, doi: 10.1029/2004JA010411, 2004.

Lockwood, M., Whiter, D., Hancock, B., Henwood, R., Ulich, T., Linthe, H. J., Clarke, E., Clilverd, M. A. The long-term drift in geomagnetic activity: Calibration of the aa index using data from a variety of magnetometer stations, Ann. Geophys., in press, 2006.

Love, J. Personal Communication, 2006.

Mayaud, P. N. Calcul preliminaire d'indices Km, Kn et Ks ou Am, An, et As, mesures de l'activité magnétique a l'échelle mondiale et dans les hémispheres Nord et Sud, Ann. Géophys.23, 585, 1967.

Mayaud, P. N. Indices Kn, Ks, et Km, 1964-67, Centre National de la Recherche Scientifique, Paris, 1968.

Mayaud, P. N. The aa index: a 100-year series characterizing the geomagnetic activity, J. Geophys. Res. 77, 6870, 1972

McPherron, R. L. Energy Input to the Magnetosphere and its Dissipation in the Ionosphere, American Geophysical Union, Fall Meeting 2004, abstract #SA13B-03, 2004.

Nevanlinna, H., Kataja, E. An extension of the geomagnetic activity index series aa for two solar cycles (1844-1868), Geophys. Res. Lett. 20(23), 2703-2706, 1993.

O'Brien, T. P., McPherron, R. L. Seasonal and diurnal variation of Dst dynamics, J. Geophys. Res. 107(A11), 1341, doi: 10.1029/2002JA009435, 2002.

Rosenberg, R. L., Coleman, P. J. Heliographic latitude dependence of dominant polarity of interplanetary magnetic field, J. Geophys.Res. 74, 5611, 1969.

Ritter, P., Lühr, H., Viljanen, A., Amm, O., Pulkkinen, A., Sillanpää, I. Ionospheric currents estimated simultaneously from CHAMP satellite and IMAGE ground-based magnetic field measurements: a statistical study at auroral latitudes, Ann. Geophys. 22(2), 417-430, 2004.

Russell, C. T. On the heliographic latitude dependence of the interplanetary magnetic field as deduced from the 22-year cycle of geomagnetic activity, Geophys. Res. Lett. 1, 11, 1974.

Russell, C. T., McPherron, R. L. Semiannual variation of geomagnetic activity, J. Geophys. Res. 78, 92, 1973.

Svalgaard, L., Geomagnetic activity: Dependence on solar wind parameters, in Coronal Holes and High Speed Wind Streams, ed. J. B. Zirker, 371, Colorado Associated University Press, Boulder, CO, 1977.

Svalgaard, L., Cliver, E. W., Ling, A. G. The semiannual variation of great geomagnetic storms, Geophys. Res. Lett. 29(16), 12, citeID 1765, doi 10.1029/2001GL014145, 2002.

Svalgaard, L., Cliver, E. W., Le Sager, P. Determination of interplanetary magnetic field strength, solar wind speed and EUV irradiance, 1890–2003, in Solar Variability as an Input to the Earth's Environment, ISCS Symp., p. 15, Eur. Space Agency, Paris, 2003.

Svalgaard, L., Cliver, E. W., Le Sager, P. IHV: A new long-term geomagnetic index, Adv. Space Res. 34(2), 436, 2004.

Svalgaard, L., Cliver, E. W. The IDV index: Its derivation and use in inferring long-term variations of the interplanetary magnetic field strength, J. Geophys. Res. 110, A12103, doi:10.1029/2005JA011203, 2005.

Svalgaard L., Cliver, E. W. Reply to the comment by M. Lockwood et al. on "The IDV index: Its derivation and use in inferring long-term variations of the interplanetary magnetic field", J. Geophys. Res. 111, A09110, doi:10.1029/2006JA011678, 2006.

Svalgaard, L., Cliver, E. W. Long-term variation of geomagnetic activity (the IHV-index) and its use in deriving solar wind speed, J. Geophys. Res. In press, doi:10.1029/2007JA012437, 2007.

Svalgaard, L., Cliver, E. W. Calibrating Sunspot Numbers Using Variations of "the Magnetic Needle", manuscript in preparation, 2007.

Wang, Y.-M., Sheeley, N. R., Jr. On the fluctuating component of the Sun's large-scale magnetic field, Ap. J. 590(2), 1111, doi: 10.1086/375026, 2003.

Figure Captions

Figure 1: Observed and reconstructed *am*-indices for Bartels rotations 2250-2255 (May 11, 1998 through Oct. 19, 1998). For every three-hour interval where solar wind data was available, *am* was computed using the relationships deduced from the analysis quoted in this paper. The scale of *am* is logarithmic because we want to verify the synthesized *am*-indices against observations over the full range of the index. The two overlapping curves (the reconstructed index is shown in red) show the two indices for times when solar wind data was available. The main area of disagreement is for very small *am*-values (e.g. for $am \leq 1$; all such cases are plotted as $am = 1$) The best-fit fourth-order polynomial is given at the bottom of the Figure.

Figure 2: Monthly averages of the *IHV*-index calculated for FRD (blue curve) compared to the monthly average *am*-index (for the same two three-hour intervals that were used for FRD) (red curve). A simple scaling (pink) of the FRD-curve makes it a very close match to the *am*-curve, showing that *IHV* from even a single station can be used as a proxy for *am*.

Figure 3: (a) Relationship between Bartels rotation means of BV_o^2 and composite *IHV* for the interval 1965-2005. (b) Comparison of computed (blue) and observed BV_o^2 (red) running 13-rotation means. Areas of consistent disagreement are marked by ovals. These occur every other solar cycle when the Rosenberg-Coleman effect is large (amplitude on arbitrary scale given by green curve).

Figure 4: Scatter-plot of yearly average *IDV* and the strength of the total interplanetary magnetic field, *B* (for all points [circles], and excluding a few outliers [small circles]), and the solar wind speed, *V* (triangles) for each

year of the interval 1965-2006. The two regression lines for *B* as a function of *IDV* give very nearly the same result within the range of the observed data points. There is no correlation (square of linear cross correlation R^2 effectively zero) between *IDV* and *V*.

Figure 5. Relationship between yearly averages of *IDV* and *Dst* using only negative *Dst*-values (Love, 2006) for the interval 1905-2004.

Figure 6: The magnitude *B* of the interplanetary magnetic field near the earth observed by spacecraft (red curve) and inferred from the *IDV*-index (blue curve and regression formula). The green curve shows *B* calculated from an extension (Love, 2006) back to 1905 of the *Dst*-index computed using only the negative values.

Figure 7: (a) Yearly means of *B* derived from *u* and *IDV* or observed by spacecraft regressed against the square root of the Zürich (International) sunspot number. (b) Variation of yearly averages since 1836 of IMF *B* inferred from Bartels' *u*-measure, the sunspot number, the *IDV*-index, and observed by spacecraft (red)

Figure 8: Because the polar cap current is fixed with respect to the sun, the earth rotates underneath the current and the magnetic effect is organized in Solar Local Time (not magnetic local time). This makes it meaningful to plot the effect in terms of its X (North) and Y (East) components (two sine curves 6 hours apart) or as a corresponding vector diagram showing the movements of the end point of the effect vector in Y-X coordinates tracing out a circular path. The Figure shows the rotation of end-point of the horizontal component vector during 1980-2004 for several stations in the Arctic polar cap: Alert (ALE), Thule (THL), Resolute Bay (RES), Cambridge Bat (CBB), and Baker Lake (BLC). For stations (ALE, THL, RES) that are well inside the auroral oval, the path is a neat circle (ALE is slightly perturbed by local induction effects) whose radius (the amplitude of the effect) is constant across the polar cap. Stations (CBB, BLC, and GJH) that are only well inside the oval part of the time show an effect that follows the nominal circular path as long as they stay inside, but are perturbed by the dayside cusp currents when not in the polar cap.

Figure 9: (a) We express the polar cap potential in terms of the solar wind electric field $\boldsymbol{V}\mathrm{x}\boldsymbol{B}$ as the product of solar wind speed *V* and magnetic field *B*. Here we show the close relationship between yearly averages of *VB* calculated from spacecraft measurements over 1965-2004 and the amplitudes of the horizontal variation for THL and for RES (there is no real difference) determining the scale factor. (b) We can then scale the geomagnetic data and compare the result with in situ space observations over the interval 1965-2006.

Figure 10: (top) Near Earth IMF strength *B* inferred from *IDV* (upper blue curve) and solar wind speed V_o (lower blue curve) computed from *IHV* and *B* compared to in situ values observed by spacecraft (red curves). (bottom) Polar cap potential BV_o calculated from the above values of *B* and V_o compared to values scaled from the amplitude of the horizontal daily variation (green curve) and observed by spacecraft (red curve).

Figure 11: Relationship between Bartels rotation averages of the *aa* -index and the global *IHV*-index for the interval 1980-2004 when there were no (known) changes to the calibration of *aa*. The relationship is slightly non-linear, so a power-law was chosen as fitting function.

Figure 12: Difference between observed and fitted *aa* during 1890-2006. After the beginning of 1957, the difference is close to zero, but at the beginning of 1957, the is a downward jump in observed *aa*-values by ~3 nT.

Figure 13: Using Helsinki (1844-1897), Wilhelmshafen (1883-1895), Batavia (1882-1894), Potsdam (1890-1907), Tokyo (1897-1912) and all available data from very many stations since 1900 we can construct a composite *IHV*-series from the present back to 1844. This Figure shows Bartels rotation averages of the composite *IHV*-index overlain by (pink curve) the 13-rotation running mean.

Figure 14: Comparison between the *aa*-index back to 1868 and the *ak*-index (red) extension thereof (derived by Nevanlinna and Kataja (1993)) and our IHV-index (blue) scaled to *aa*. The *ak*-values are generally ~6 nT lower.

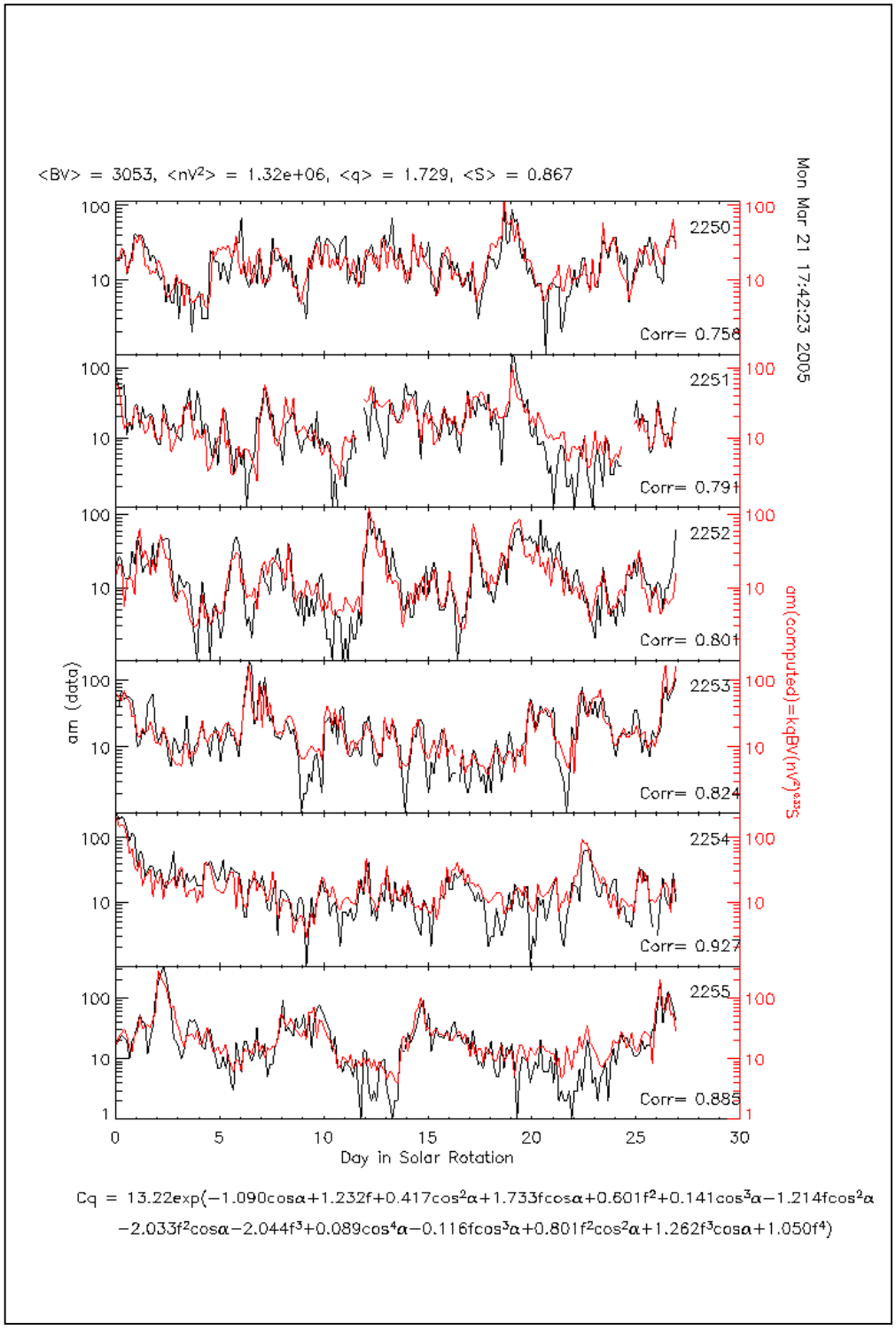
<BV> = 3053, <nV²> = 1.32e+06, <q> = 1.729, <S> = 0.867
Mon Mar 21 17:42:23 2005
2250
Corr= 0.758
2251
Corr= 0.791
2252
Corr= 0.801
2253
Corr= 0.824
2254
Corr= 0.927
2255
Corr= 0.885
am (data)
am(computed)=kqBV(nV²)^a S^s
Day in Solar Rotation
Cq = 13.22exp(−1.090cosα+1.232f+0.417cos²α+1.733fcosα+0.601f²+0.141cos³α−1.214fcos²α
−2.033f²cosα−2.044f³+0.089cos⁴α−0.116fcos³α+0.801f²cos²α+1.262f³cosα+1.050f⁴)

Figure 1

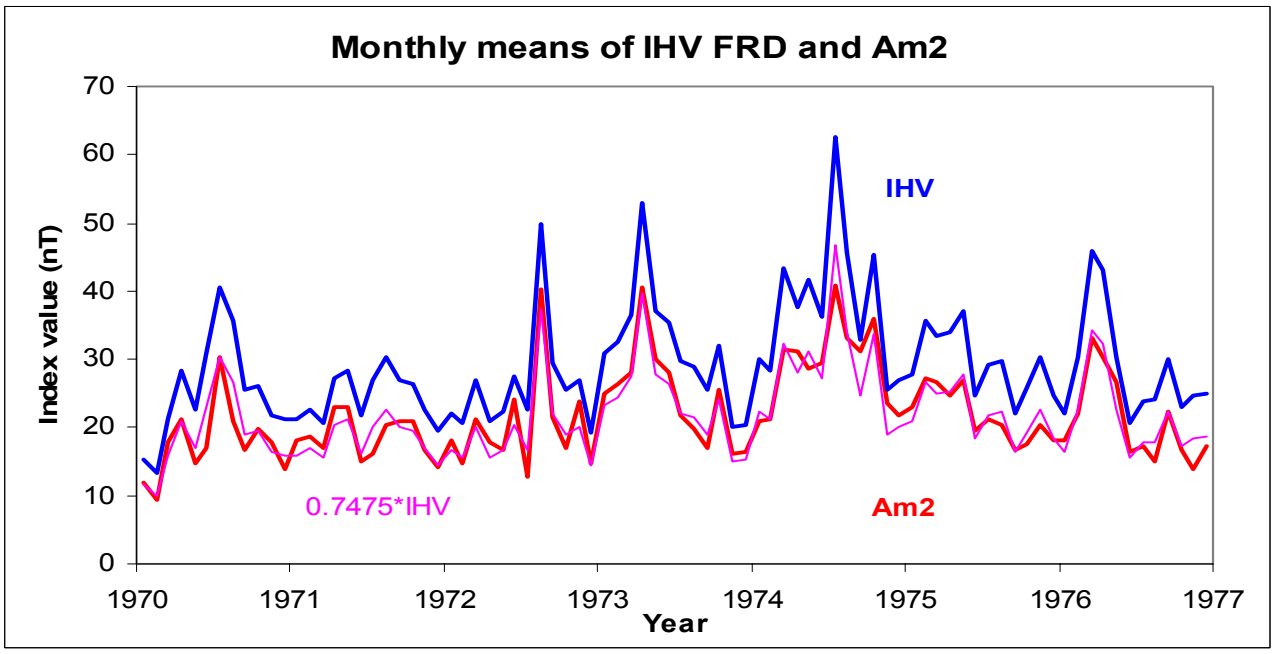

Figure 2

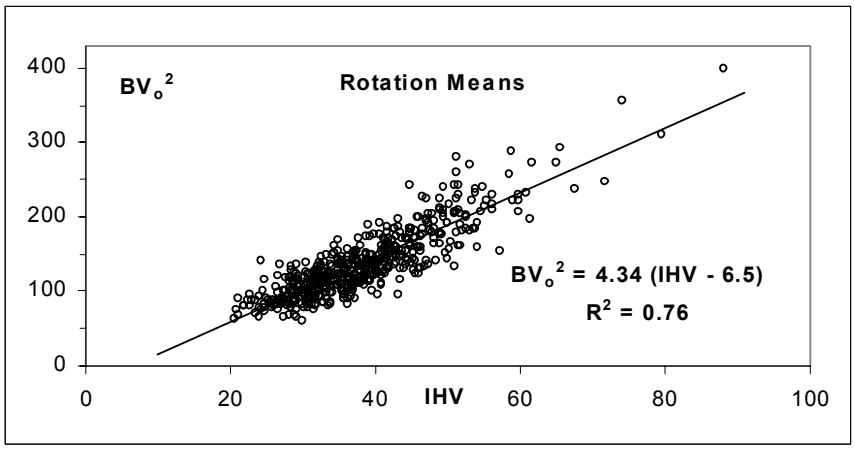

Figure 3a

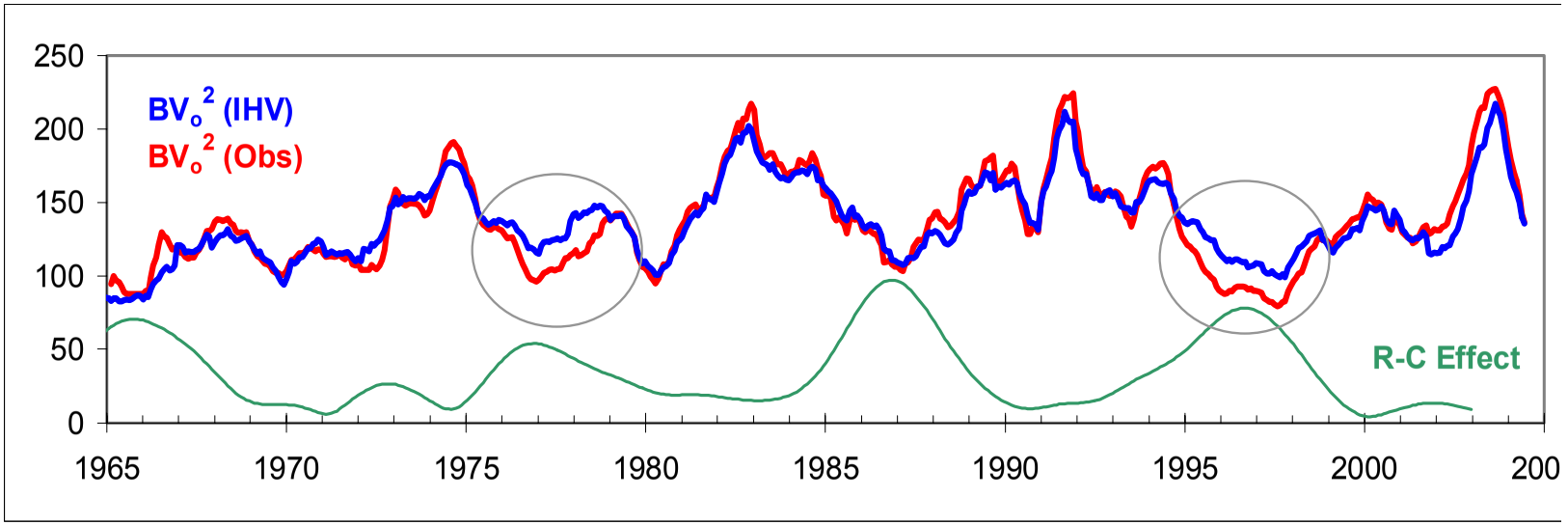

Figure 3b

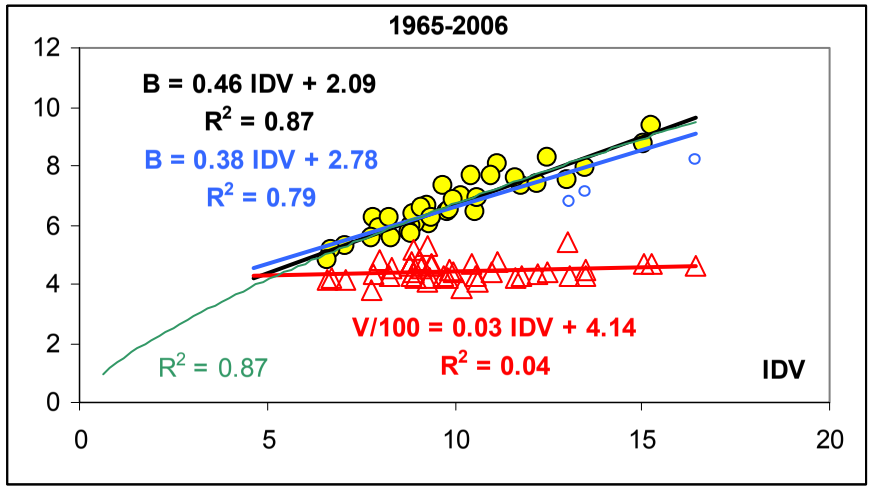

Figure 4

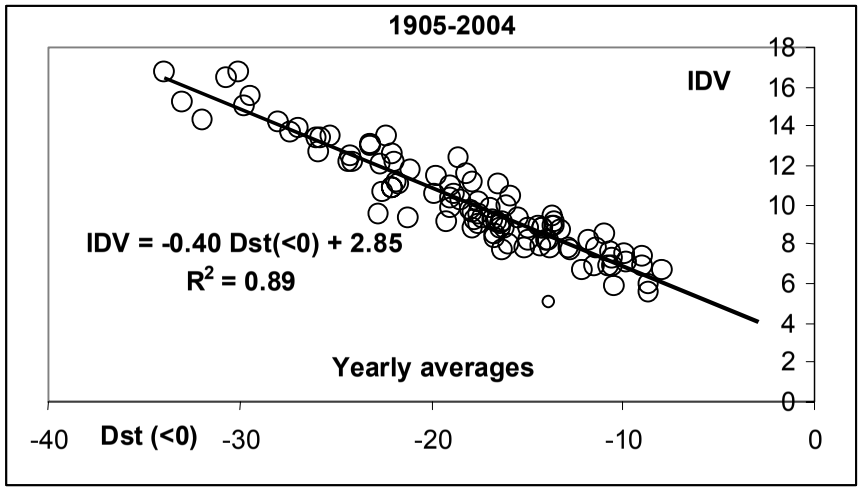

Figure 5

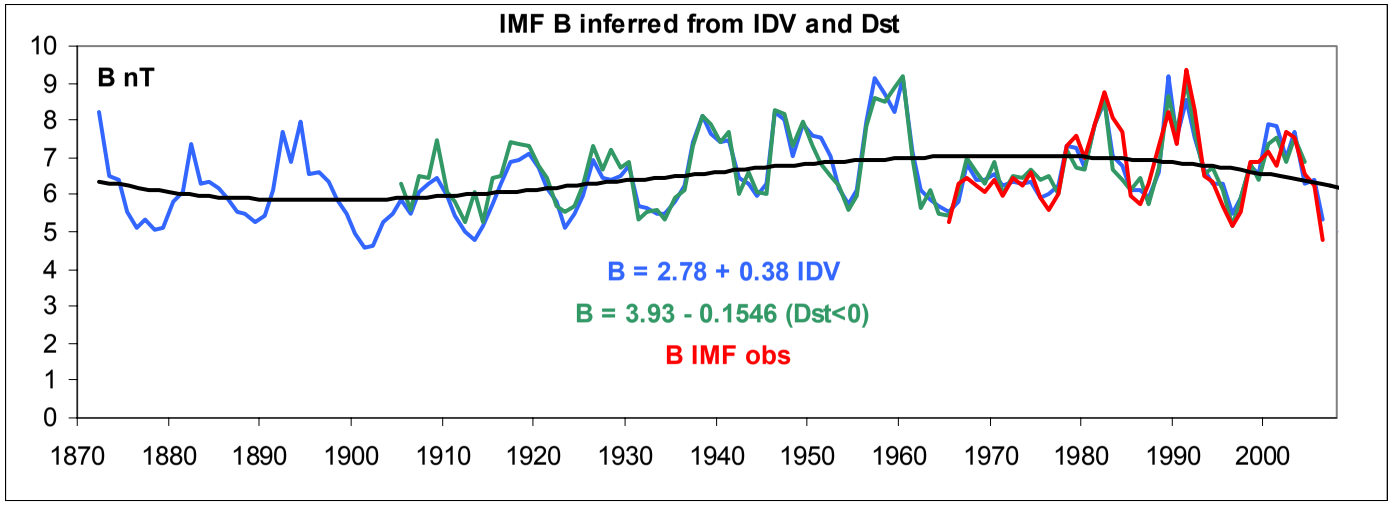

Figure 6

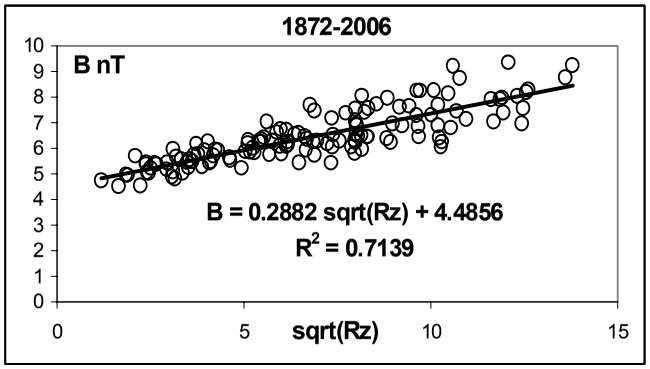

Figure 7a

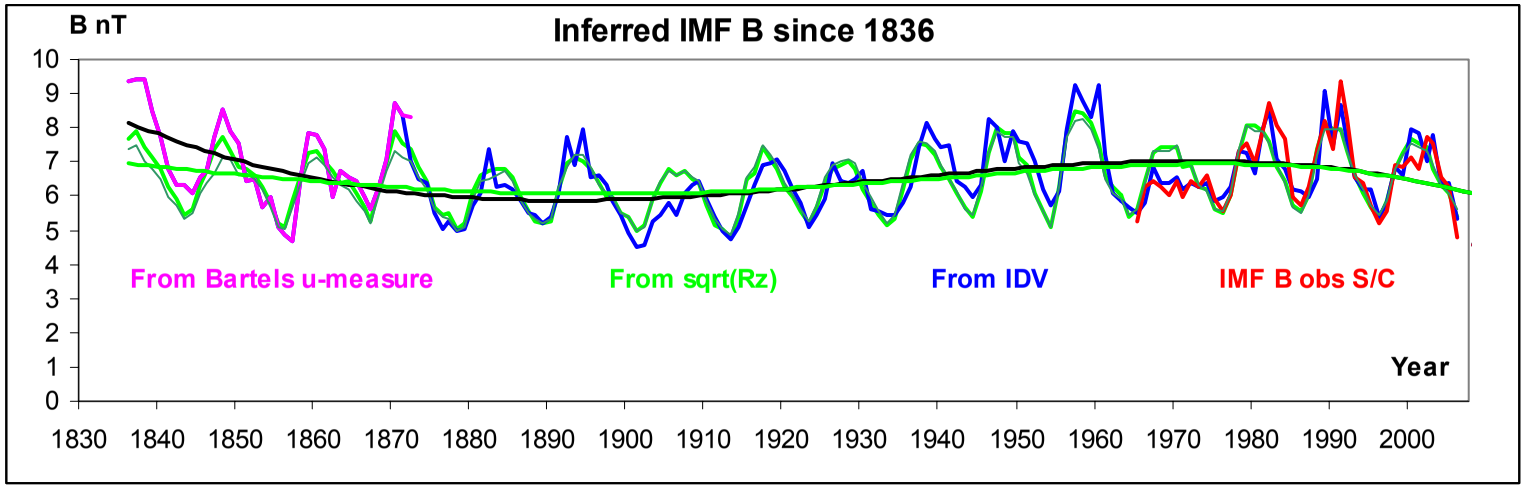

Figure 7b

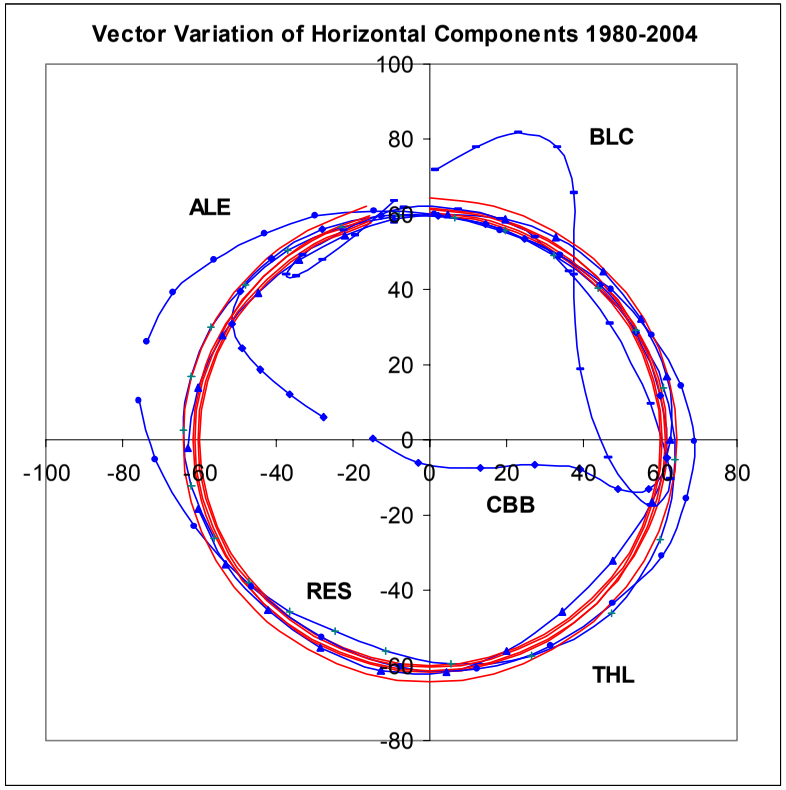
Vector Variation of Horizontal Components 1980-2004
100
80
60
40
20
0
-20
-40
-60
-80
-100
-80
-60
-40
-20
0
20
40
60
80
BLC
ALE
CBB
RES
THL

Figure 8

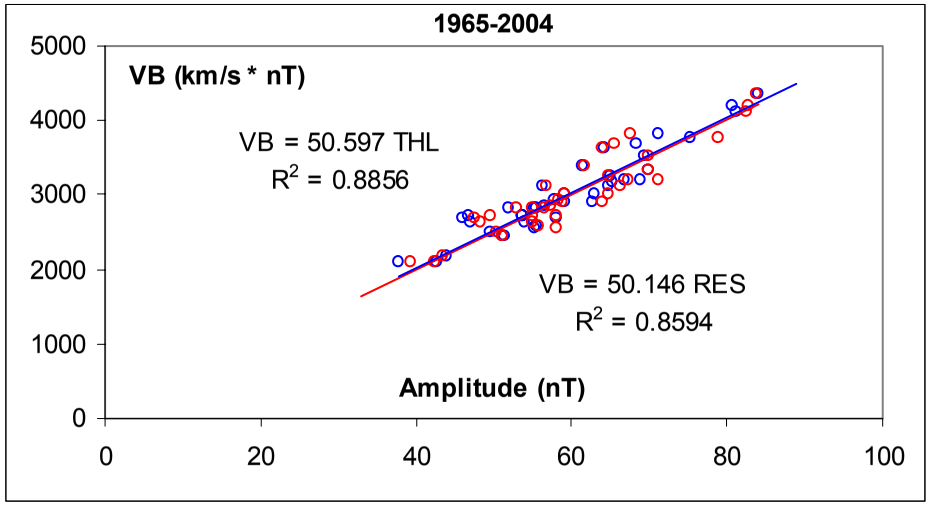

Figure 9a

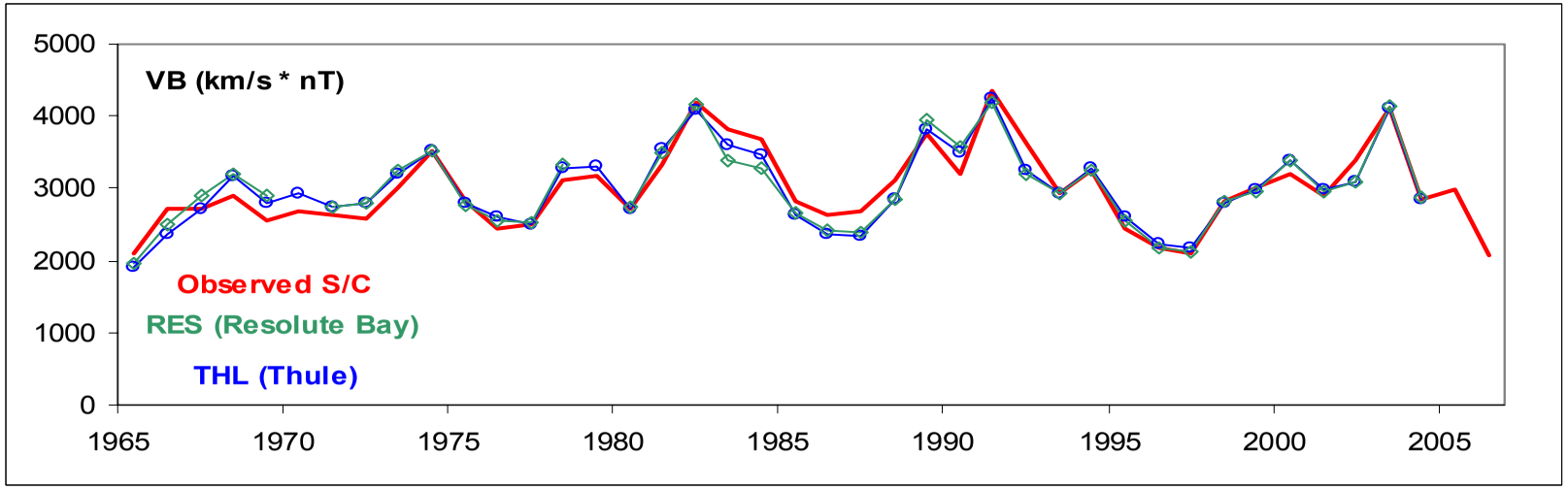

Figure 9b

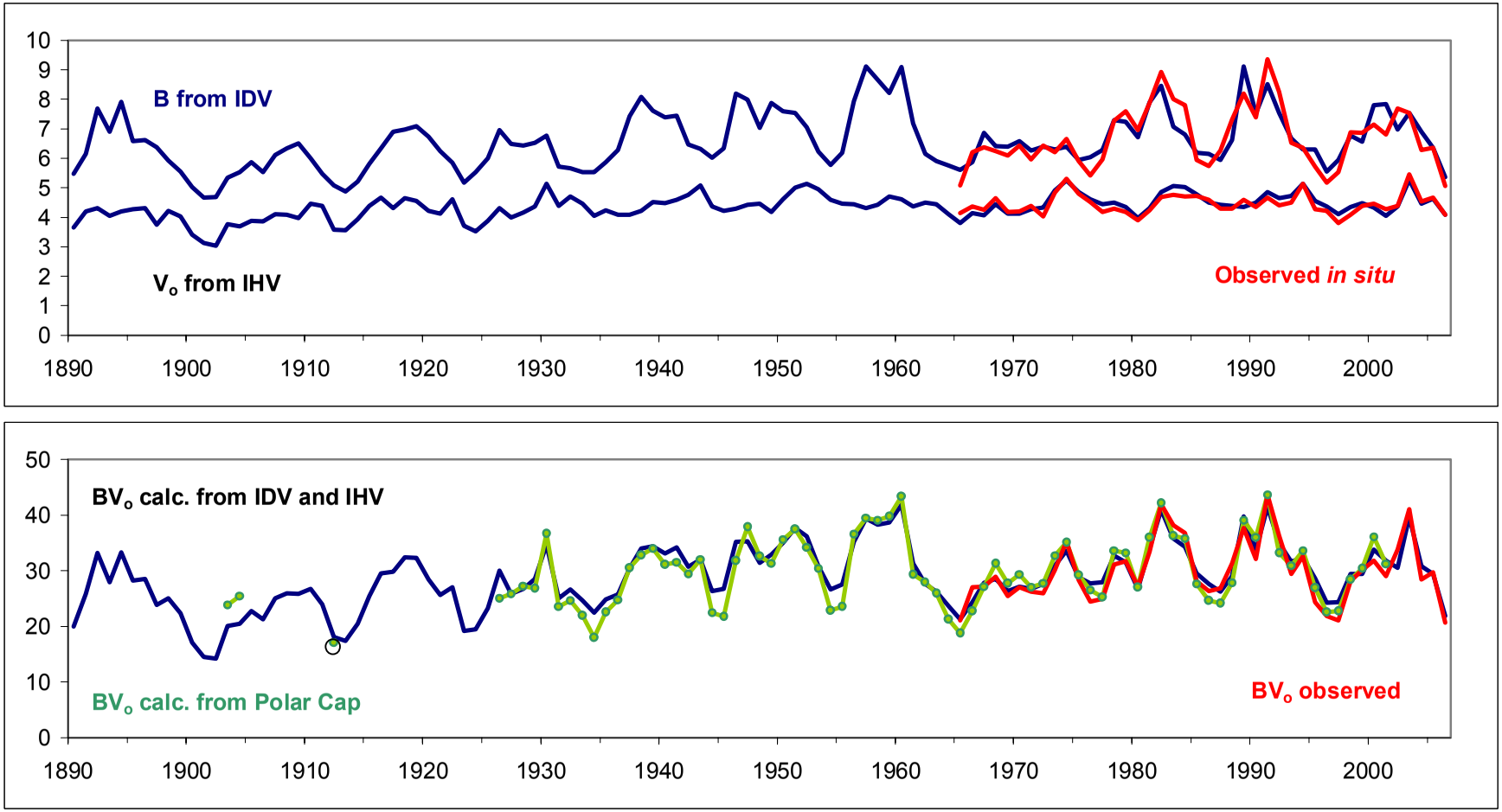
B from IDV
V_o from IHV
Observed *in situ*
BV_o calc. from IDV and IHV
BV_o calc. from Polar Cap
BV_o observed
1890
1900
1910
1920
1930
1940
1950
1960
1970
1980
1990
2000

Figure 10

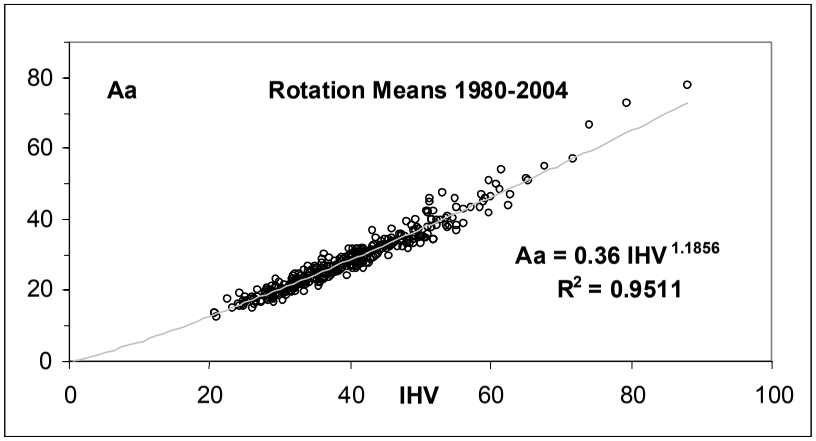

Figure 11

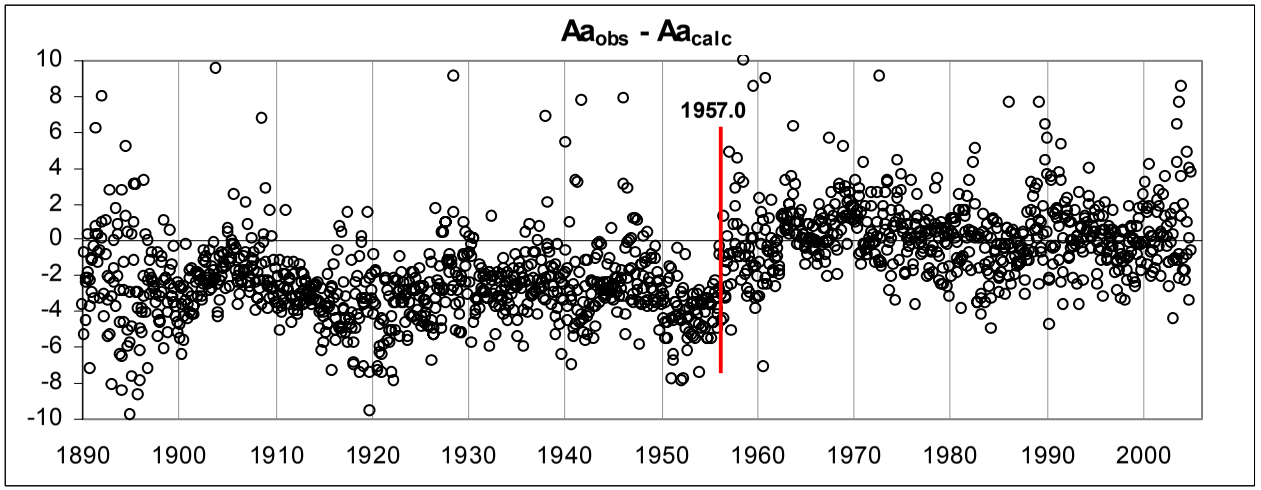

Figure 12

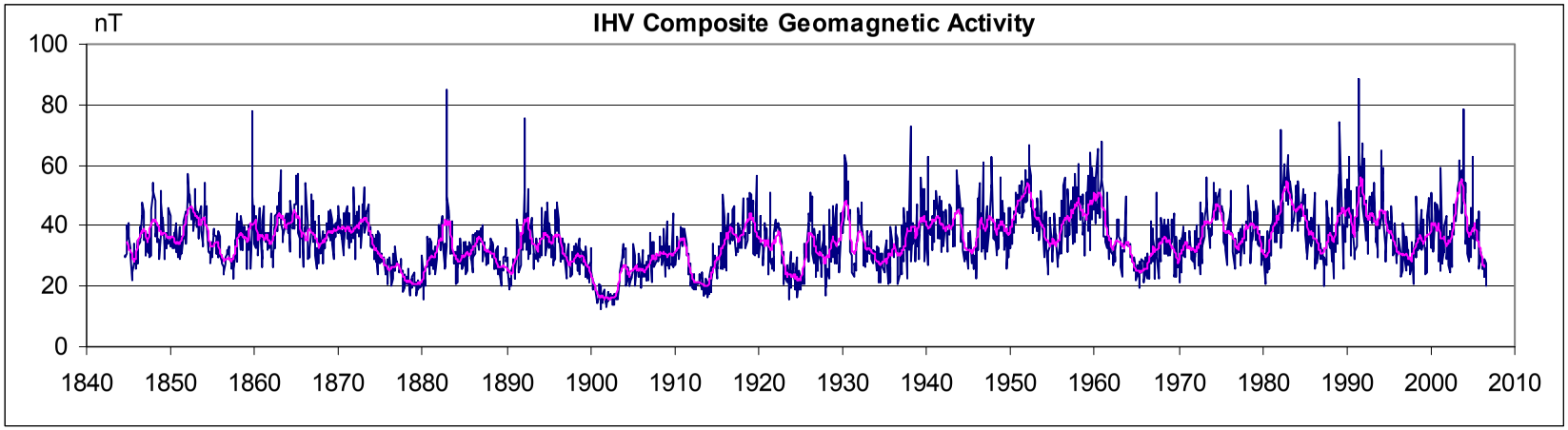

Figure 13

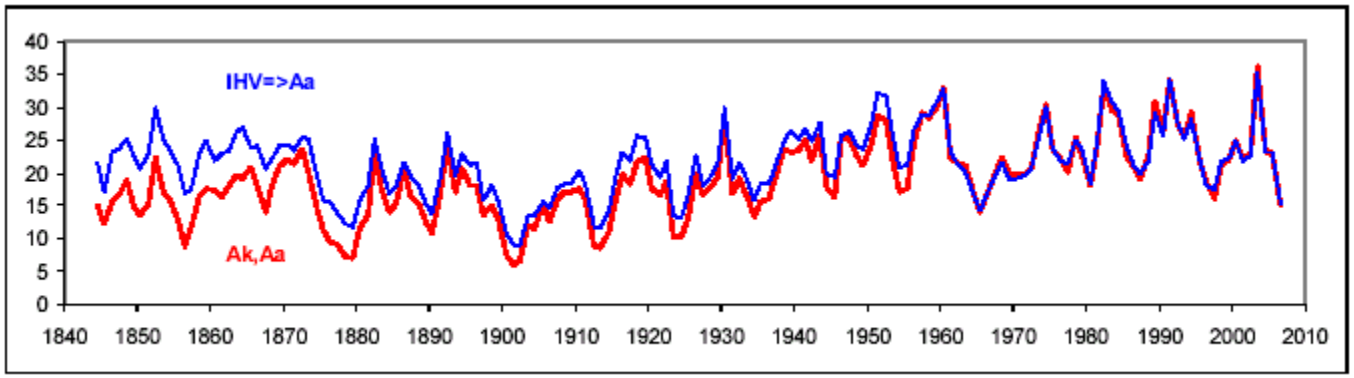

Figure 14